

## Theory of all-optical switching based on the Kerr nonlinearity in metallic nanohybrids

Mahi R. Singh \*

*Department of Physics and Astronomy, The University of Western Ontario, London, Canada N6A 3K7*

 (Received 16 December 2019; revised 7 May 2020; accepted 9 June 2020; published 7 July 2020)

We have developed a theory for the Kerr nonlinearity in nanohybrids made of an ensemble of metallic nanoshells and low concentration of quantum emitters. A metallic nanoshell is made of a metallic core sphere and dielectric shell. We consider that quantum emitters are four-level quantum systems. When a probe laser light falls in the metallic nanoshells, the surface plasmon polariton electric field is produced at the interface between the metal sphere and dielectric shell. This electric field along with the probe field induces dipoles in metallic nanoshells. These dipoles interact with each other via the dipole-dipole interaction. The Kerr nonlinearity has been calculated by using the quantum density matrix method in the presence of the dipole-dipole interaction (coupling). We found that in the weak-coupling limit there is an enhancement in the Kerr nonlinearity. On the other hand, in the strong-coupling limit, the peaks in the Kerr coefficient split from two peaks to four peaks when the frequency of the dipole electric field is in the resonance with the exciton frequency. The splitting in the spectrum is due to the presence of the dressed states created in the system. We showed that heights and locations of peaks are very sensitive to the strength of the dipole-dipole interaction. Physics of the enhancement can be used to fabricate Kerr nanosensors. On the other hand, physics of the splitting from two peaks (ON) to four peaks (OFF) can be used to fabricate Kerr nanoswitches.

DOI: [10.1103/PhysRevA.102.013708](https://doi.org/10.1103/PhysRevA.102.013708)

### I. INTRODUCTION

Considerable interest has been devoted to study linear and nonlinear plasmonic properties of nanohybrids and nanocomposites made of metallic nanoparticles (MNPs) and quantum emitters (QEs) [1–19]. It is well known that nonlinear optics play an important role in various applications such as frequency conversion [11], ultrafast lasers and amplifiers [12], ultrafast all-optical switching [13], and nonlinear microscopy [14]. Strong laser intensities are required in various nonlinear optical applications. Recently it has been found that surface plasmon polaritons (SPPs) in metallic nanoparticles create huge electric fields near the surfaces of MNPs [1–10]. Therefore, SPP fields instead of strong laser intensities can be used for various nonlinear optical applications. The nonlinear optical properties of quantum emitters near the MNPs has been studied by several authors [7,15–19]. For example, plasmonic excitations have been studied for ultrafast processing of optical signals which depend on the size and the shape of the MNPs along with dielectric properties of the surrounding medium [18]. Singh [19] studied the nonlinear second-harmonic generation in nanohybrids made of the MNP and quantum dot (QD). It is found that second-harmonic signals produced by the QD near the MNP are enhanced due to the exciton-SPP interaction.

Nonlinear optical phenomena called the Kerr nonlinearity has been studied widely in the research area of quantum optics using three-level and four-level atoms [20–29]. For example, Schmidt and Imamoglu [20] have obtained giant

Kerr nonlinearities in atoms by electromagnetically induced transparency. Wang *et al.* [21] found that the Kerr nonlinear refractive index of a three-level  $\Lambda$ -type atom is greatly enhanced inside an optical ring cavity near resonance for both probe and control fields. On the other hand, Yan *et al.* [22] investigated the enhancement of the Kerr nonlinearity in a four-level atomic system in which spontaneously generated coherence is present. Wang *et al.* [23] studied experimentally the enhancement of the Kerr-nonlinear coefficient in a three-level atomic system such as Rb atom for various coupling beam powers.

Some effort has also been devoted to investigating experimentally the Kerr nonlinearity in metallic nanohybrids [28,29]. For example, Torres-Torres *et al.* [28] have studied the third-order optical nonlinearity a nanohybrid containing gold nanoparticles and silicon quantum dots nucleated by ion implantation in a high-purity silica matrix. On the other hand, López-Suárez *et al.* [29] studied nonlinear refractive index for three different systems made of high-purity silica substrates with silicon quantum dots (QDs), silver metallic nanoparticles (Ag MNPs). They used a femtosecond optical Kerr gate with 80-fs pulses at 830 nm to investigate the magnitude and response time of their nonlinear response. They found that the inclusion of Ag-MNP enhances the nonlinearity of the nanohybrid by a factor of around 3. They also found that the confinement effect of the Si QDs in the sample plays an important role for the excitation of the SPP resonance related to the Ag MNPs.

In this paper, we developed a theory of the Kerr nonlinearity in nanohybrids made of an ensemble of QEs doped in an ensemble of metallic nanoshells (MNSs). The MNS is made of a metallic core sphere and dielectric shell. The concentration of QEs is small so that they do not interact with

\*msingh@uwo.ca

each other. On the other hand, the concentration of MNSs is large and they interact with each other via the dipole-dipole interaction (DDI). A probe field is applied to study the Kerr nonlinearity. The probe field and the SPP field induce dipoles in the ensemble of MNSs and they interact with each other via DDI.

Recently, Singh and Black [30] have studied the effect of the DDI on the one-photon photoluminescence in a core-shell nano hybrid where the core is made of a metallic nanoparticle and the shell is made of an ensemble of QEs. They found that this DDI between QEs plays a dominant role in the phenomenon of the one-photon photoluminescence and scattering cross section. Later, Singh and co-workers [31,32] have discovered the anomalous one-photon photoluminescence quenching in metallic nano hybrids due to the DDI. They found that their theory is consistent with the experiments of metallic nano hybrids made from the CdSe-ZnS quantum dot embedded in the ensemble of Au nanoparticles.

Here we consider four energy levels of QEs in the nano hybrid. This means that each QE has three excitation and four energy levels. The excitons in QEs interact with the SPP field and DDI field produced by the ensemble of MNSs. A theory of the Kerr nonlinearity has been developed by using the quantum density-matrix method in the presence of the exciton-SPP and exciton-DDI interactions (coupling). Analytical expressions of the Kerr refractive index coefficient have been evaluated in the weak- and strong-coupling limits of the exciton-SPP and exciton-DDI interactions.

We found that in the weak-coupling limit, there is enhancement in the Kerr nonlinearity coefficient. On the other hand, in the strong-coupling limit, the peaks in the Kerr coefficient splits from two peak to four peaks. The splitting in the spectrum is due to the presence of the dressed states in the nano hybrid due the strong interaction when the frequencies of the SSP and field are resonant with the exciton's energies. On the hand when the frequencies of the SSP and DDI fields are *not* resonant with the exciton's frequencies, two peaks of the Kerr coefficient split into more than four peaks. We showed that the height and locations of these peaks are very sensitive to the DDI coupling.

## II. DIPOLE-DIPOLE INTERACTION HAMILTONIAN

The nano hybrid is made of interacting MNSs and noninteracting QEs. We consider only four levels of QEs and they are called four-level systems in the literature [20–24]. Four levels are denoted as  $|1\rangle$ ,  $|2\rangle$ ,  $|3\rangle$ , and  $|4\rangle$  and the frequency difference between levels  $|i\rangle$  and  $|j\rangle$  is expressed as  $\omega_{ij}$  where  $i$  and  $j$  stand for 1, 2, 3, and 4. A schematic diagram of the QEs and MNSs hybrid is depicted in Fig. 1. To study the Kerr nonlinearity, we apply a probe field with amplitude  $E_P$  and frequency  $\omega$  between the transitions  $|1\rangle \leftrightarrow |2\rangle$ . The MNS emits the surface plasmon polaritons electric fields  $E_{SPP}$ . The induced dipoles are created due to the probe field and SPP field in MNSs and they interact with each other via the DDI. The induced dipole also creates the DDI electric field which is denoted as  $E_{DDI}^m$ .

To study the nonlinear optical properties of QEs, we must calculate how many electric fields are falling on the QE. The answer is that there are three electric fields falling on the QE.

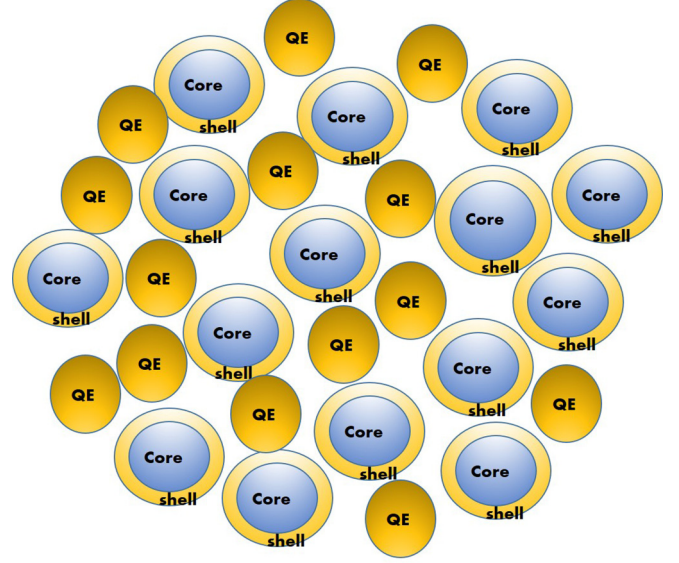


FIG. 1. Schematic diagram of a hybrid which consists of an ensemble of interacting MNSs and noninteracting QEs. The MNS is made of a dielectric shell and a metallic core. The hybrid is doped into a chemical, dielectric, or biological material.

They are (i) probe electric field  $E_P$ , (ii) the SPP field  $E_{SPP}$ , and (3) the DDI field  $E_{DDI}^m$ . Therefore, the total electric field falling on the QE is found as

$$E_q^T = (E_P + E_{SPP} + E_{DDI}^m). \quad (1)$$

Let us calculate the SPP field and the DDI field appearing in Eq. (1).

*SPP field.* A MNS is made from a metallic core and a dielectric shell. The SPP field is calculated as follows. The dielectric constant of the metallic core and dielectric shell are denoted as  $\epsilon_m$  and  $\epsilon_s$ , respectively. The radius of the metallic core is taken as  $R_m$  and the radius of the dielectric shell is  $R_s$ . The nano hybrid is deposited on a substrate (i.e., background material) with dielectric constant  $\epsilon_b$ . The background material can be the chemical, biological dielectric materials or solutions or solids. We applied a probe field with frequency  $\omega_p$  and amplitude  $E_P$  in the nano hybrid. Induced dipoles are created in MNSs and QEs.

The dipole of the MNS is denoted as  $P_m$  which produces the SPP electric field  $E_{SPP}$ . Two electric fields are falling on the MNS, namely the probe field and the electric field produced by induced dipole in the QE ( $E_{QE}$ ). Then, the total electric field falling on the MNS is found as  $E_T^m = E_P + E_{QE}$ . Using this total field and solving the Maxwell's equation in the quasistatic approximation [33,34] one can find the following expressions  $E_{SPP}$  as

$$E_{SPP} = \frac{P_m}{4\pi\epsilon_0\epsilon_b r^3}, \quad P_m = 4\pi\epsilon_0\epsilon_b R_s^3 g_l \zeta_s (E_P + E_{QE}),$$

$$\zeta_s = \left[ \frac{\epsilon_{mc} - \epsilon_b}{\epsilon_{mc} + 2\epsilon_b} \right], \quad \epsilon_{mc} = \epsilon_m \left[ \frac{R_s^3 + R_m^3 \left( \frac{\epsilon_m - \epsilon_s}{\epsilon_m + 2\epsilon_s} \right)}{R_s^3 - 2R_m^3 \left( \frac{\epsilon_m - \epsilon_s}{\epsilon_m + 2\epsilon_s} \right)} \right], \quad (2)$$

where  $\zeta_s$  is called the polarizability factor. Similarly, one can calculate the electric fields  $E_{QE}$  produced by the induced dipole  $P_q$  in the QE. Three electric fields are falling on the QE, namely the probe field, the SPP field, and the DDI electric field produced by the MNPs. Then, the total electric field falling on the QE is found as in Eq. (1). Solving the Maxwell's equations in the quasistatic approximation [33,34] one can find the following expressions  $E_{QE}$  as

$$\begin{aligned} E_{QE} &= \frac{P_q}{4\pi\epsilon_0\epsilon_b r^3}, \\ P_q &= 4\pi\epsilon_0\epsilon_b R_q^3 g_l \zeta_q (E_P + E_{SPP} + E_{DDI}^m), \\ \zeta_q &= \left[ \frac{\epsilon_q - \epsilon_b}{\epsilon_q + 2\epsilon_b} \right]. \end{aligned} \quad (3)$$

In Eqs. (2) and (3), the constant  $g_l$  is called the polarization parameter and it has values  $g_l = 1$  and  $g_l = -2$  for  $\mathbf{P}_i \parallel \mathbf{E}_P$  and  $\mathbf{P}_i \perp \mathbf{E}_P$  where  $i = m, q$ .

Equations (2) and (3) can be rewritten in the simple form as follows:

$$E_{SPP} = \frac{R_s^3 \beta_m}{r^3} (E_P + E_{QE}), \quad \beta_m = g_l \zeta_s, \quad (4)$$

$$E_{QE} = \frac{R_q^3 \beta_q}{r^3} (E_P + E_{SPP} + E_{DDI}^m) \quad \beta_q = g_l \zeta_q. \quad (5)$$

Note that both electric fields depend on  $r^{-3}$  and parameters  $\beta_s$  and  $\beta_q$ .

*DDI field.* Let us calculate the DDI field produced by the ensemble of MNSs in the nanohybrid. Each dipole in the ensemble interacts with other dipoles. A theory of the DDI has been developed in Refs. [30–32] and the DDI electric field is found as

$$E_{DDI}^m = \frac{\lambda P_m}{(3 \times 4\pi\epsilon_0\epsilon_b) R_s^3}, \quad (6)$$

where  $\lambda$  is a constant and  $P_m$  is the polarization which has been calculated in Eq. (2). Putting the expression of  $P_m$  from Eq. (2) into Eq. (6) and performing some mathematical manipulations, one can calculate the DDI field as

$$E_{DDI}^m = \eta_{DDI}^m E_P + \eta_{DDI}^m \left( \frac{R_q^3 \beta_q}{r^3} E_P + \frac{R_s^3 \beta_m \beta_q}{r^6} E_P \right), \quad (7)$$

where  $\eta_{DDI}^m$  is the DDI strength and is found as

$$\eta_{DDI}^m = \frac{\lambda g_l \zeta_s}{3} = \frac{\lambda \beta_m}{3}. \quad (8)$$

Note that the second term in Eq. (7) depends on  $r^{-3}$  and  $r^{-6}$ .

Putting Eqs. (5) and (7) into Eq. (4), we can calculate the SPP field as follows:

$$E_{SPP} = \frac{R_s^3 \beta_m}{r^3} \left( E_P + \eta_{DDI}^m E_P + \frac{R_q^3 \beta_q}{r^3} E_P \right). \quad (9)$$

Note that the SPP and DDI fields depend on  $r^{-3}$  and  $r^{-6}$ . The higher-order terms ( $r^{-9}$ ) has been neglected.

The SSP resonance frequencies are calculate from Eq. (4). Note that SSP field in Eq. (4) depends on the  $\zeta_s$  function which

has a maximum which corresponds to the SPP resonance frequency. The SPP resonance frequency is located at the interface between the core and metallic shell and is denoted by  $\omega_s$ .

### III. KERR NONLINEAR PLASMONICS AND DENSITY-MATRIX METHOD

In this section we calculate the nonlinear Kerr coefficient using the density-matrix method. Using the quantum-mechanical density-matrix method, nonlinear optical properties in quantum optics been have studied in Refs. [35,36]. To study the nonlinear properties in the QE, we applied a probe electric field ( $E_P$ ) with frequency  $\omega_p$  between the transition  $|1\rangle \leftrightarrow |2\rangle$ . Following the method of Refs. [35,36], the expression of the polarization  $P_{QE}$  is given as

$$P_{QE}(\omega_p) = P_{QE}^{(2)}(\omega_p) + P_{QE}^{(2)}(\omega_p, \omega_p) + P_{QE}^{(3)}(\omega_p, \omega_p, \omega_p), \quad (10)$$

where

$$\begin{aligned} P_{QE}^{(1)}(\omega_p) &= \epsilon_0 \chi_{QE}^{(1)}(\omega_p) E_P(\omega_p), \\ P_{QE}^{(2)}(\omega_p, \omega_p) &= \epsilon_0 \chi_{QE}^{(2)}(\omega_p, \omega_p) E_P(\omega_p) E_P(\omega_p), \\ P_{QE}^{(3)}(\omega_p, \omega_p, \omega_p) &= \epsilon_0 \chi_{QE}^{(3)}(\omega_p, \omega_p, \omega_p) E_P(\omega_p) E_P(\omega_p) E_P(\omega_p), \end{aligned} \quad (11)$$

where  $\chi^{(1)}$ ,  $\chi^{(2)}$ , and  $\chi^{(3)}$  are the first-, second-, and third-order expressions of the susceptibility  $\chi$ . We know that the first-order susceptibility is responsible for the one-photon phenomena, whereas the second-order susceptibility is responsible for the two-photon phenomena. Finally, the third-order susceptibility is responsible for the Kerr nonlinearity.

Following the method of Refs. [35–38], the polarization of the QE can also be expressed in terms of the quantum density-matrix operator ( $\rho$ ) as follows:

$$P_{QE}(\omega_p) = 2\mu_{21} [\rho_{21}(\omega_p) + \text{H.c.}], \quad (12)$$

where  $\mu_{21}$  is the matrix elements of the dipole moment between the transition  $|1\rangle \leftrightarrow |2\rangle$  and  $\rho_{21}$  is the nonlinear density-matrix operator ( $\rho$ ) between the transition  $|1\rangle \leftrightarrow |2\rangle$ . We express the nonlinear density matrix as follows:

$$\rho_{21} = \rho_{21}^{(1)}(\omega_p) + \rho_{21}^{(2)}(\omega_p, \omega_p) + \rho_{21}^{(3)}(\omega_p, \omega_p, \omega_p), \quad (13)$$

where  $\rho_{21}^{(1)}$ ,  $\rho_{21}^{(2)}$ , and  $\rho_{21}^{(3)}$  are the first-, second-, and third-order density-matrix elements in the probe field, respectively. Putting Eq. (13) into Eq. (12), we get

$$\begin{aligned} P_{QE}(\omega_p) &= 2\mu_{21} [\rho_{21}^{(1)}(\omega_p) + \rho_{21}^{(2)}(\omega_p, \omega_p) \\ &\quad + \rho_{21}^{(3)}(\omega_p, \omega_p, \omega_p) + \text{H.c.}]. \end{aligned} \quad (14)$$

We compared Eqs. (10) and (14) and we found the relation between the susceptibility and the density-matrix elements as

follows:

$$\begin{aligned}\chi^{(1)}(\omega_p) &= \frac{2\mu_{21}\rho_{21}^{(1)}(\omega_p) + \text{H.c.}}{\epsilon_0 E_p(\omega_p)}, \\ \chi^{(2)}(\omega_p, \omega_p) &= \frac{2\mu_{21}\rho_{21}^{(2)}(\omega_p, \omega_p) + \text{H.c.}}{\epsilon_0 E_p(\omega_p) E_p(\omega_p)}, \\ \chi^{(3)}(\omega_p, \omega_p, \omega_p) &= \frac{2\mu_{21}\rho_{21}^{(3)}(\omega_p, \omega_p, \omega_p) + \text{H.c.}}{\epsilon_0 E_p(\omega_p) E_p(\omega_p) E_p(\omega_p)}.\end{aligned}\quad (15)$$

The above expression can be expressed in terms of the Rabi frequency as

$$\begin{aligned}\chi^{(1)}(\omega_p) &= \frac{2\mu_{21}^2 \rho_{21}^{(1)}(\omega_p) + \text{H.c.}}{\epsilon_0 \hbar \Omega_p}, \\ \chi^{(2)}(\omega_p, \omega_p) &= \frac{2\mu_{21}^3 \rho_{21}^{(2)}(\omega_p, \omega_p) + \text{H.c.}}{\epsilon_0 \hbar^2 \Omega_p^2}, \\ \chi^{(3)}(\omega_p, \omega_p, \omega_p) &= \frac{2\mu_{21}^4 \rho_{21}^{(3)}(\omega_p, \omega_p, \omega_p) + \text{H.c.}}{\epsilon_0 \hbar^3 \Omega_p^3}.\end{aligned}\quad (16)$$

In this paper, we are interested to study the effect of Kerr effect on plasmonic properties of metallic nanohybrids. Therefore, here we consider only the third-order susceptibility  $\chi^{(3)}$  which is responsible for the Kerr effect.

Next, we calculate the Kerr refractive index coefficient (i.e., Kerr coefficient). It can be calculated from the following formula [35,36]:

$$n_2 = \frac{12\pi^2 \text{Re}(\chi^{(3)})}{n_b^2 c}, \quad (17)$$

where  $n_b$  is the refractive index of the background material and  $c$  is the speed of the light. Putting in the expression of the third-order susceptibility  $\chi^{(3)}$  from Eq. (16) into Eq. (17), we get

$$n_2 = n_2^0 \text{Re}(\rho_{21}^{(3)}), \quad n_2^0 = \frac{12\pi^2 2\mu_{21}^4}{n_b^2 c \epsilon_0 \hbar^3 \Omega_p^3}. \quad (18)$$

Note that the Kerr nonlinearity coefficient depends on the third-order density-matrix element  $\rho_{21}^{(3)}$ . Next using the quantum density-matrix method, we evaluate these density-matrix elements.

#### IV. KERR COEFFICIENT AND DENSITY-MATRIX METHOD

Let us evaluate an expression of density-matrix element  $\rho_{21}^{(3)}$  appearing in Eq. (18). To evaluate this density matrix, we need to calculate the interaction Hamiltonian between excitons in the QE and the ensemble of MNSs. To calculate the interaction Hamiltonian, first we must calculate the total electric field falling on the QE. We applied a probe electric field ( $E_p$ ) between the transition  $|1\rangle \leftrightarrow |2\rangle$ . We consider that the  $\omega_s$  lies near exciton energy  $\omega_{23}$ . Hence the SPP field is acting between the transition  $|2\rangle \leftrightarrow |3\rangle$ . The DDI field is acting between the transition  $|3\rangle \leftrightarrow |4\rangle$ . See the schematic diagram of the QE in Fig. 2. The total electric field falling on the QE is obtained by putting Eqs. (7) and (9) into Eq. (1)

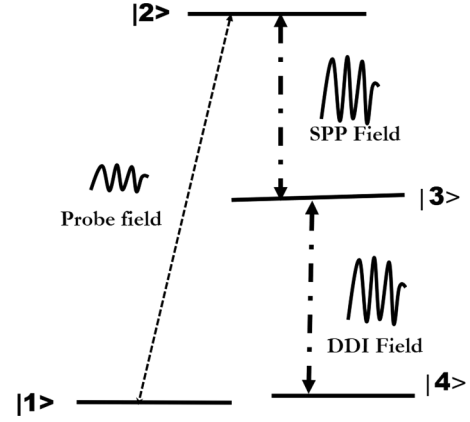


FIG. 2. A schematic diagram of a four-level QE is plotted. Energy levels are denoted as  $|1\rangle$ ,  $|2\rangle$ ,  $|3\rangle$ , and  $|4\rangle$ . The probe field is applied between transitions  $|1\rangle \leftrightarrow |2\rangle$ . The SPP field and DDI field are acting between  $|2\rangle \leftrightarrow |3\rangle$  and  $|3\rangle \leftrightarrow |4\rangle$ , respectively.

as follows:

$$E_q^T = \begin{bmatrix} (E_p + \eta_{\text{DDI}}^m E_p) \\ + \left( \frac{R_s^3 \beta_m}{r^3} + \frac{R_s^3 \beta_m \eta_{\text{DDI}}^m}{r^3} + \frac{R_q^3 \beta_q \eta_{\text{DDI}}^m}{r^3} \right) E_p \\ + \left( \frac{R_s^3 R_s^3 \beta_m \beta_q}{r^6} + \frac{R_q^3 R_s^3 \beta_m \beta_q \eta_{\text{DDI}}^m}{r^6} \right) E_p \end{bmatrix}. \quad (19)$$

These electric fields induce the dipole in the QE and this dipole in turn interacts with these fields. With the help of Eq. (19) and using the dipole and rotating wave approximation [35–38], the interaction Hamiltonian is found as follows:

$$H_{\text{in}} = \begin{bmatrix} \hbar \Omega_p \sigma_{21} + \hbar \Omega_p (\eta_{\text{DDI}}^m + \Lambda_{\text{DDI}}^q + \Lambda_{\text{DDI}}^{qm}) E \sigma_{34} \\ + \hbar \Omega_p (\Pi_{\text{SPP}}^p + \Pi_{\text{SPP}}^{ddi} + \Pi_{\text{SPP}}^{qe}) \sigma_{23} + \text{H.c.} \end{bmatrix}, \quad (20)$$

where

$$\begin{aligned}\Lambda_{\text{DDI}} &= (\eta_{\text{DDI}}^m + \Lambda_{\text{DDI}}^q + \Lambda_{\text{DDI}}^{qm}), \\ \Pi_{\text{SPP}} &= (\Pi_{\text{SPP}}^p + \Pi_{\text{SPP}}^{ddi} + \Pi_{\text{SPP}}^q), \\ \eta_{\text{DDI}}^m &= \frac{\lambda \beta_m}{3}, \quad \Lambda_{\text{DDI}}^q = \frac{R_q^3 \beta_q \eta_{\text{DDI}}^m}{r^3}, \\ \Lambda_{\text{DDI}}^{qm} &= \frac{R_q^3 R_s^3 \beta_m \beta_q \eta_{\text{DDI}}^m}{r^6}, \quad \Pi_{\text{SPP}}^p = \frac{R_s^3 \beta_m}{r^3}, \\ \Pi_{\text{SPP}}^{ddi} &= \frac{R_s^3 \beta_m \eta_{\text{DDI}}^m}{r^3}, \quad \Pi_{\text{SPP}}^q = \frac{R_q^3 R_s^3 \beta_m \beta_q}{r^6},\end{aligned}\quad (21)$$

where H.c. stands for the Hermitian conjugate. Here  $\sigma_{ij} = |i\rangle\langle j|$  is the exciton creation operator for  $|i\rangle \leftrightarrow |j\rangle$ . The parameter  $\Omega_p$  is called the Rabi frequency. The first term in the Hamiltonian is the exciton-probe field interaction due to the transitions  $|2\rangle \leftrightarrow |1\rangle$ . The second term is the exciton-DDI field interactions due to the transitions  $|3\rangle \leftrightarrow |4\rangle$ . The third term is the exciton interaction with SPP field. The last term is the exciton-SPP field interaction due to the transitions  $|2\rangle \leftrightarrow |3\rangle$ .

Note that the DDI term ( $\Lambda_{\text{DDI}}$ ) in Eq. (21) is made of three terms. The first term is the exciton-DDI field interaction term. On the other hand, the second and third terms are the exciton interaction with the DDI field induced by the QE electric field. Similarly, the SPP term ( $\Pi_{\text{SPP}}$ ) in Eq. (21) is made of three

terms. The first term is the exciton interaction with SPP field induced by the probe field. However, the second term is the exciton interaction with the SPP field induced by the DDI electric field. On the other hand, the third term is the exciton interaction with the SPP field induced by the QE electric field.

$$\rho_{12}^{(3)} = \frac{\rho_{23}^{(2)} \Omega_p^2 \Pi_{\text{SPP}} d_{14} + i \rho_{24}^{(2)} \Omega_p^2 \Lambda_{\text{DDI}} \Pi_{\text{SPP}}}{d_{21} (d_{13} d_{14} - d_{21} \Omega_p^2 \Lambda_{\text{DDI}}^2) + \Omega_p^2 \Pi_{\text{SPP}}^2 d_{14}} + \frac{i(\rho_{22}^{(2)} - \rho_{11}^{(2)}) \Omega_p (d_{13} d_{14} - d_{21} \Omega_p^2 \Pi_{\text{SPP}}^2)}{d_{21} (d_{13} d_{14} - d_{21} \Omega_p^2 \Lambda_{\text{DDI}}^2) + \Omega_p^2 \Pi_{\text{SPP}}^2 d_{14}}, \quad (22)$$

where

$$\begin{aligned} d_{31} &= \delta_p + i\gamma_{31}, & d_{32} &= \delta_s + i\gamma_{32}, & d_{21} &= \delta_{21} + i\gamma_{21}, \\ d_{43} &= \delta_{43} + i\gamma_{43}, & d_{41} &= \delta_{41} + i\gamma_{41}, & d_{42} &= \delta_{42} + i\gamma_{42}, \\ \delta_p &= \omega_p - \omega_{31}, & \delta_s &= \omega_{sp} - \omega_{32}, & \delta_d &= \omega_{sp} - \omega_{43}, \\ \delta_{41} &= \delta_p + \delta_d, & \delta_{12} &= \delta_s - \delta_p, & \delta_{42} &= \delta_d + \delta_s, \end{aligned}$$

where  $\delta_p$ ,  $\delta_s$ , and  $\delta_d$  are the probe, SPP, and DDI detunings, respectively. In Eq. (22)  $\rho_{23}^{(2)}$ ,  $\rho_{23}^{(2)}$ ,  $\rho_{22}^{(2)}$ ,  $\rho_{12}^{(1)}$ ,  $\rho_{13}^{(1)}$ , and  $\rho_{23}^{(2)}$  are the matrix elements of the density-matrix operator  $\rho$ . They are found as

$$\begin{aligned} \rho_{24}^{(2)} &= -\frac{i\rho_{23}^{(2)} \Omega_p \Pi_{\text{SPP}} d_{34}}{d_{24} d_{34} + \Omega_p^2 \Lambda_{\text{DDI}}^2}, \\ \rho_{22}^{(2)} &= \frac{\Omega_p \text{Im}(\rho_{12}^{(1)})}{\gamma_{21}}, \\ \rho_{13}^{(1)} &= -\left( \frac{d_{14} \Lambda_{\text{DDI}} \Omega_p^2}{d_{21} (d_{13} d_{14} - \Omega_p^2 \Pi_{\text{SPP}}^2) + d_{14} \Omega_p^2 \Lambda_{\text{DDI}}^2} \right), \\ \rho_{23}^{(2)} &= \frac{(i\rho_{33}^{(2)} \Omega_p \Lambda_{\text{DDI}} - i\rho_{22}^{(2)} \Omega_p \Lambda_{\text{DDI}} + i\rho_{13}^{(1)} \Omega_p) (d_{24} d_{34} + \Omega_p^2 \Lambda_{\text{DDI}}^2)}{(d_{24} d_{34} + \Omega_p^2 \Lambda_{\text{DDI}}^2) + \Omega_p^2 \Pi_{\text{SPP}}^2 d_{34}}. \end{aligned} \quad (23)$$

If we consider that the population of the ground state is higher than the population all excited states. In other words, we can put  $\rho_{11} > \rho_{22}$ ,  $\rho_{11} > \rho_{22}$ ,  $\rho_{11} > \rho_{33}$ , and  $\rho_{11} > \rho_{44}$ . In this case the expression of  $\rho_{12}^{(3)}$  reduces to

$$\rho_{12}^{(3)} = \frac{\rho_{23}^{(2)} \Omega_p^2 \Pi_{\text{SPP}} d_{14} + i \rho_{24}^{(2)} \Omega_p^3 \Lambda_{\text{DDI}} \Pi_{\text{SPP}}}{d_{21} (d_{13} d_{14} - d_{21} \Omega_p^2 \Lambda_{\text{DDI}}^2) + \Omega_p^2 \Pi_{\text{SPP}}^2 d_{14}}, \quad (24)$$

where

$$\begin{aligned} \rho_{24}^{(2)} &= -\frac{i\rho_{23}^{(2)} \Lambda_{\text{DDI}} d_{34}}{d_{24} d_{34} + \Pi_{\text{SPP}}^2}, \\ \rho_{23}^{(2)} &= \frac{(i\rho_{13}^{(1)} \Omega_p) (d_{24} d_{34} + \Pi_{\text{SPP}}^2)}{d_{23} (d_{24} d_{34} + \Pi_{\text{SPP}}^2) + \Lambda_{\text{DDI}}^2 d_{34}}. \end{aligned} \quad (25)$$

The Kerr coefficient appearing in Eq. (18) can be calculated with the help of  $\rho_{12}^{(3)}$  which is calculated in this section.

## V. RESULTS AND DISCUSSIONS

In this section, we calculate the Kerr coefficient using our theory. We consider that a nanohybrid is made of an ensemble of interacting MNSs and noninteracting QEs. The MNS is made of the SiO<sub>2</sub> shell and a gold (Au) core. Cadmium-selenium quantum dots are considered as QEs. This type of nanohybrids are fabricated by Xiao *et al.* [39]. We consider the following expression of the dielectric constant of the

Following the method of Refs. [35–38] and with the help of Hamiltonian Eq. (21), equations of motion for density-matrix elements are evaluated. We solve density-matrix element equations in the steady state. After some mathematical manipulations, the density-matrix element  $\rho_{12}^{(3)}$  is calculated as follows:

metal  $\epsilon_m$ :

$$\epsilon_m = \epsilon_\infty \left( 1 - \frac{\omega_p^2}{\omega^2 + i\gamma_c \omega} \right), \quad (26)$$

where  $\epsilon_\infty$  is the dielectric constant of metal when the light frequency is very large,  $\omega_p$  is the plasmon frequency (wavelength), and  $\gamma_m$  is the decay constant responsible for the heat loss in metals. The experimental parameters for the Au are taken as  $\omega_p = 8.7$  eV,  $\gamma_m = 0.1$  eV, and  $\epsilon_\infty = 10$ . Other physical parameters are measured with respect to the decay rate  $\gamma_0$  in the vacuum. The parameters used are  $\gamma_{23} = \gamma_{34} = \gamma_0$ ,  $\gamma_{12} = 0.2\gamma_0$ , and  $\Omega_p = 0.2\gamma_0$ .

Now, we study the influence of the DDI on Kerr nonlinearity in the weak SPP coupling limit. Physical parameters such as probe Rabi frequency, probe detuning, and decay rates are measured with respect to the decay rate  $\gamma_0$ . In the weak limit we take  $\Pi_{\text{SPP}} = 0.1$ . The variation of Kerr nonlinear coefficient  $n_2$  is plotted in Fig. 3(a) versus probe detuning  $\delta_p$ . The probe field is taken as  $\Omega_p = 0.1$ . Here we consider that the DDI and SPP resonance frequencies are in resonance with the exciton transition energies  $\omega_{34}$  and  $\omega_{23}$ , respectively. The solid line is plotted when the DDI is absent ( $\Lambda_{\text{DDI}} = 0.0$ ). The dash and dash-dotted lines are plotted in the presence of the DDI for  $\Lambda_{\text{DDI}} = 0.3$ , and  $\Lambda_{\text{DDI}} = 0.6$ , respectively. It is clear from the figure that the shape of the Kerr coefficient changes in the presence of the DDI. Note that there is a huge

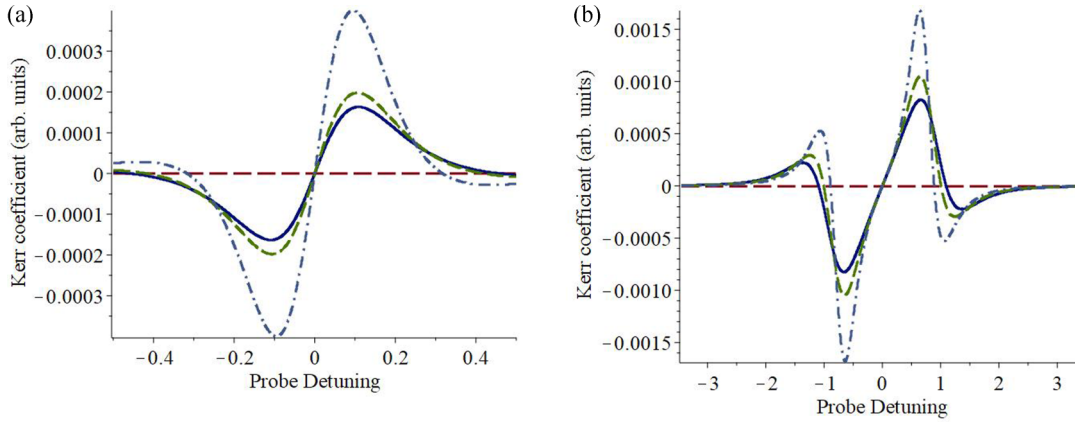


FIG. 3. (a) In the weak-coupling limit ( $\Pi_{\text{SPP}} = 0.1$ ), the Kerr nonlinear coefficient  $n_2$  is plotted as a function of the probe detuning  $\delta_p$ . The solid line is plotted when the DDI is absent ( $\Lambda_{\text{DDI}} = 0.0$ ). The dash and dash-dotted lines are plotted in the presence of the DDI for  $\Lambda_{\text{DDI}} = 0.3$ , and  $\Lambda_{\text{DDI}} = 0.6$ , respectively. (b) In the strong-coupling limit ( $\Pi_{\text{SPP}} = 2.0$ ), the Kerr nonlinear coefficient  $n_2$  is plotted as a function of the probe detuning  $\delta_p$ . The solid line is plotted in the absence of the DDI. The dash and dash-dotted lines are plotted for the DDI when the anomalous DDI has values  $\Lambda_{\text{DDI}} = 0.5$ , and  $\Lambda_{\text{DDI}} = 0.8$ , respectively.

enhancement of the Kerr coefficient under the presence of the anomalous DDI effect. The Kerr coefficient changes from the negative to positive value at zero detuning, i.e.,  $\delta_p = 0$ . The positions of the left peak and the right peak located on both sides of the zero detuning do not change. The distance of the left peak and the right peak from the zero detuning is the same.

We study the effect of the DDI on the Kerr coefficient in the strong-coupling limit ( $\Pi_{\text{SPP}} = 2.0$ ). The results are presented in Fig. 3(b) for  $n_2$  as a function of the probe detuning  $\delta_p$ . The solid line is plotted in the absence the DDI. The dash and dash-dotted lines are plotted for the DDI when the anomalous DDI has values  $\Lambda_{\text{DDI}} = 0.5$ , and  $\Lambda_{\text{DDI}} = 0.8$ , respectively. The Kerr coefficient changes from positive to negative at  $\delta_p = -2.0$ . It also changes from negative to positive value at  $\delta_p = 0.0$  and from positive to negative at  $\delta_p = +2.0$ . This means that the transition point at  $\delta_p = 0.0$  splits into two transition points located at  $\delta_p = -2.0$  and  $\delta_p = +2.0$ . In other words, the left minimum peak in the Kerr coefficient in the absence of the SSP coupling splits into two minima which are located on the left and right side of zero detuning. Similarly, the right maximum peak splits into two peaks which are located on the left and right side of zero detuning.

Note that in Fig 3(b), the splitting distance between  $\delta_p = 0.0$  and  $\delta_p = \mp 2.0$  is equal to the SSP coupling value which is  $\Pi_{\text{SPP}} = 2.0$ . The height of the left peak is the same as the height of the right peak. However, the height of the left and right peaks located at  $\delta_p = \mp 2.0$  are not the same. There is again a huge enhancement of the Kerr coefficient under the presence of the SSP field and a small enhancement in the presence of the DDI. In summary, we can say that two peaks in the Kerr coefficient split into four peaks in the strong SPP coupling limit.

We want to explain the physics of the splitting in Fig. 3(b). In the weak SPP coupling limit, the Kerr coefficient has two peaks at the right side and the left side of the zero detuning. This peak is associated with the transition  $|2\rangle \leftrightarrow |1\rangle$ . On the other hand, in the strong SPP coupling limit, the Kerr coefficient has two peaks at the right side and two peaks at the left side of the zero detuning. In this case, dressed states are

created in the QEs. The excited state  $|2\rangle$  splits into two dressed states called  $|2_{-}\rangle$  and  $|2_{+}\rangle$  due to the strong SPP coupling. Therefore, two transitions occur,  $|2_{-}\rangle \leftrightarrow |1\rangle$  and  $|2_{+}\rangle \leftrightarrow |1\rangle$ . Due to transition  $|2_{-}\rangle \leftrightarrow |1\rangle$ , we get the first set of two left and right peaks. Similarly, due to the transition  $|2_{+}\rangle \leftrightarrow |1\rangle$ , we get the second set of the two left and right peaks. That is why we get four peaks in the strong-coupling limit.

The effect of DDI is studied in Fig. 4 on the left and right peaks of the Kerr effect. We know that the left and right peaks in the absence of the DDI are located at  $\delta_p = -0.1$  and  $\delta_p = +0.1$ , respectively [see Fig. 3(a)]. In Fig 4, the peak heights are plotted as a function of the DDI coupling. The solid line is plotted for the right peak at  $\delta_p = +0.1$  and the dash-dotted line is plotted for the left peak at  $\delta_p = -0.1$ . Note that the enhancement in the Kerr coefficient in the both peaks increases then reaches the maximum value at about  $\Lambda_{\text{DDI}} = 0.90$ . After that both peaks have zero values about  $\Lambda_{\text{DDI}} = 0.95$  and after this value both peaks change their sign.

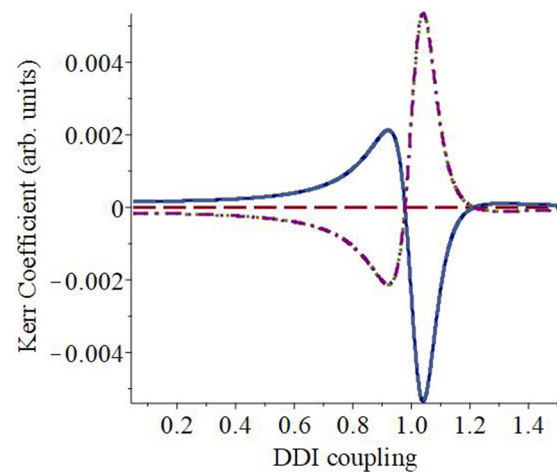


FIG. 4. The Kerr coefficient ( $n_2$ ) as function of the anomalous DDI ( $\Lambda_{\text{DDI}}$ ) is plotted. The solid and dotted lines correspond to  $\delta_p = +0.1$  and  $\delta_p = -0.1$ , respectively.

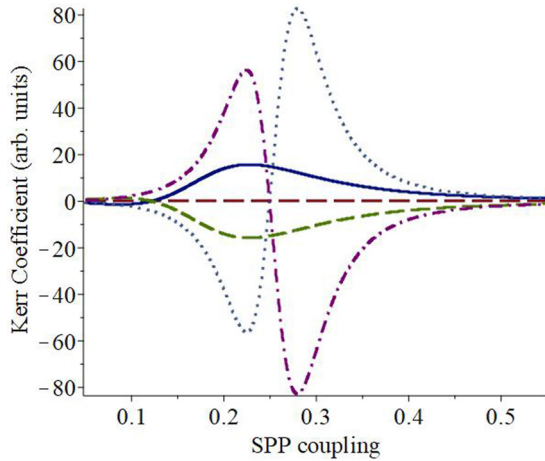


FIG. 5. The Kerr coefficient ( $n_2$ ) peaks heights are plotted as a function of the SPP coupling ( $\Pi_{\text{SPP}}$ ). The solid line ( $\delta_p = +0.1$ ) and the dashed line ( $\delta_p = -0.1$ ) are plotted for  $\Lambda_{\text{DDI}} = 0.99$ . The dash-dotted line ( $\delta_p = +0.1$ ) and the dotted line ( $\delta_p = -0.1$ ) are plotted for  $\Lambda_{\text{DDI}} = 1.0$ .

The right peak changes sign from positive to negative (see the solid curve) and the left peak changes sign from negative to positive (see the dash-dotted curve).

The value of the DDI at which the Kerr coefficient changes sign is called the critical DDI value and it is denoted as  $\Lambda_{\text{DDI}}^{\text{crit}}$ . For Fig. 4, the critical DDI value is  $\Lambda_{\text{DDI}}^{\text{crit}} = 0.95$ . It is found that the DDI critical value depends on the intensity of the DDI and SSP couplings. One can say that with small variation of the DDI the Kerr coefficient can be switched from the positive to negative value (ON) to the negative to positive value (OFF). This means that the present hybrid can be used for the fabrication of all-switch nanodevices.

In Fig 5, we study the effect of the DDI when the SSP strength is varied. The Kerr coefficient is plotted as a function of the SPP coupling. The solid line is for the right ( $\delta_p = +0.1$ ) and the dashed line for the left peak ( $\delta_p = -0.1$ ). We consider the value of the DDI coupling as  $\Lambda_{\text{DDI}} = 0.99$ . Now we increase the value of the DDI coupling slightly to  $\Lambda_{\text{DDI}} = 1.0$ . In this case the dash-dotted line is for the right peak and the dotted line is for the left peak. One can see that heights of peaks for the solid and dashed curves increase with the SSP coupling until about  $\Pi_{\text{SPP}} = 1.0$  and then they decrease. On the other hand, the dotted and dash-dotted curves have similar behaviour as Fig. 4(a) except that the right peak and the left peak have opposite sign. In summary, we conclude that one can switch the magnitude of the Kerr nonlinear coefficient from positive (ON) to negative value (OFF) by tuning the intensity of the anomalous DDI. This means one can fabricate the all-optical nanoswitching devices using these nanohybrids.

Here, we study the DDI effect on the Kerr coefficient by varying the SPP detuning ( $\delta_s$ ). We plot the Kerr coefficient as a function of the SPP detuning in Fig. 6. The solid, dash, and dash-dotted lines correspond to  $\Lambda_{\text{DDI}} = 0.44$ ,  $\Lambda_{\text{DDI}} = 0.5$ , and  $\Lambda_{\text{DDI}} = 0.54$ , respectively. The value of the SSP coupling is taken as  $\Pi_{\text{SPP}} = 0.99$ . Note that for these values of parameters, the Kerr coefficient changes sign three times (see

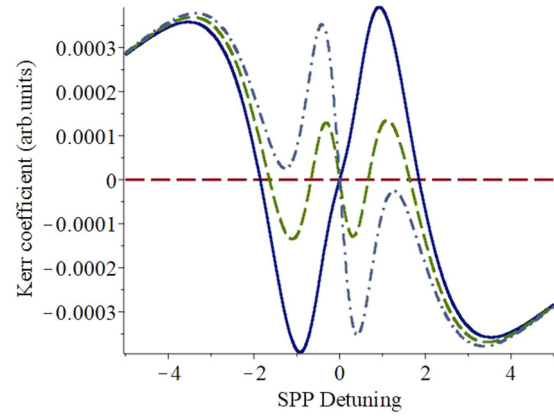


FIG. 6. The Kerr coefficient ( $n_2$ ) is plotted as a function of the SPP detuning ( $\delta_s$ ). The solid, dash, dash-dotted lines correspond to  $\Lambda_{\text{DDI}} = 0.44$ ,  $\Lambda_{\text{DDI}} = 0.5$ , and  $\Lambda_{\text{DDI}} = 0.54$ , respectively. The value of the SPP coupling is taken as  $\Pi_{\text{SPP}} = 0.99$ .

solid curve) when the DDI coupling is  $\Lambda_{\text{DDI}} = 0.44$ . When we change slightly the DDI coupling to  $\Lambda_{\text{DDI}} = 0.5$ , the Kerr coefficient changes sign five times (see dotted curve). Finally, when we change slightly the DDI coupling to  $\Lambda_{\text{DDI}} = 0.54$ , the Kerr effect changes sign only one time (see dash-dotted curve). Similarly, by fixing the DDI coupling and varying the SSP coupling, we found a similar effect as found in Fig. 5. This means by choosing the suitable values of the SSP coupling and varying the DDI coupling the Kerr coefficient changes sign from one to three to five times. This mechanism can be used to fabricate all-optical nanoswitches.

Further, in Fig. 7, the effect of the DDI detuning ( $\delta_d$ ) on the Kerr coefficient has been investigated. The Kerr coefficient is plotted as a function of the DDI detuning. The solid and dash-dotted lines correspond to  $\Pi_{\text{SPP}} = 0.2$  and  $\Pi_{\text{SPP}} = 0.8$ , respectively. The value of the DDI coupling is taken as  $\Lambda_{\text{DDI}} = 0.5$ . Note that in the weak SPP coupling limit ( $\Pi_{\text{SPP}} = 0.2$ ) the Kerr effect changes sign one time (see solid curve). On the other hand, in the strong SPP coupling limit ( $\Pi_{\text{SPP}} = 0.8$ ) the Kerr effect changes sign *three* times (see

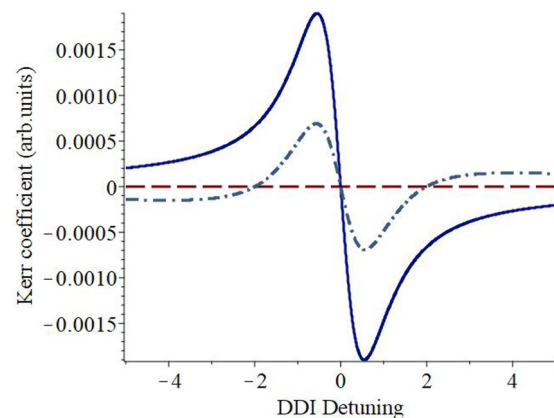


FIG. 7. The Kerr coefficient ( $n_2$ ) is plotted as a function of the DDI detuning ( $\delta_d$ ). The solid and dash-dotted lines correspond to  $\Pi_{\text{SPP}} = 0.2$  and  $\Pi_{\text{SPP}} = 0.8$ , respectively. The value of the DDI coupling is taken as  $\Lambda_{\text{DDI}} = 0.5$ .

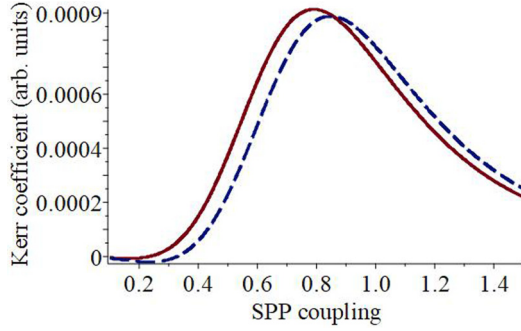


FIG. 8. The Kerr coefficient ( $n_2$ ) is plotted as a function of the SPP coupling ( $\Pi_{\text{SPP}}$ ). The solid and dotted lines are plotted for  $\delta_p = 0.50$  and  $\delta_p = 0.55$ , respectively.

dash-dotted curve). The change of sign from one time to three times is due to the dressed states created in the system as we explained in Fig. 3(b).

We also found that if we keep the SSP coupling in the weak limit (i.e.,  $\Pi_{\text{SPP}} = 0.2$ ) and the DDI coupling in the strong limit (i.e.,  $\Lambda_{\text{DDI}} = 2.0$ ), the Kerr effect does not change sign from one to three times, but changes sign only one time. The figure is not included here. This is because the Kerr coefficient is due to the transition  $|2\rangle \leftrightarrow |1\rangle$ . The strong DDI coupling is acting in the transition  $|3\rangle \leftrightarrow |4\rangle$ . Therefore, strong DDI coupling does not create dressed states in the transition  $|2\rangle \leftrightarrow |1\rangle$  since it is acting in the transition  $|3\rangle \leftrightarrow |4\rangle$ . There is no splitting in the right and left peaks of the Kerr coefficient as we found Fig. 3(b) and that is why the curve changes one time.

Next, we investigated the effect of the SPP coupling on the Kerr effect. Recently Tohari *et al.* [16] have done very interesting work to study the effect of the Kerr nonlinearity on a nanohybrid made of a metallic nanosphere, a quantum dot, and a graphene nanorod. They have investigated the effect of the SPP coupling on the Kerr nonlinearity. In their paper they called the SPP coupling the local field effect. They found an enhancement in the Kerr absorption spectrum due to the presence of SPP field created by the metallic nanosphere and the graphene nanorod. It is important to note that their model is very different than our model. We have plotted the effect of the SPP coupling in Fig. 8. In this figure, the Kerr coefficient is plotted as a function of the SPP coupling for varying the probe field. The DDI coupling is taken as  $\Lambda_{\text{DDI}} = 0.1$ . The solid line is plotted for the probe detuning  $\delta_p = 0.50$  and the dash line is plotted for the probe detuning  $\delta_p = 0.55$ . One can see from Fig. 8 that in the weak SPP coupling limit (i.e.,  $\Pi_{\text{SPP}} < 1.0$ ) the Kerr coefficient increases. After a certain value of the SPP coupling it reaches maximum value and then it decreases in the strong SPP coupling limit (i.e.,  $\Pi_{\text{SPP}} > 1.0$ ). This behavior can be understood from the density matrix  $\rho_{21}^{(3)}$  given by Eq. (24). Note that SPP coupling appears in the numerator and denominator in Eq. (24). In the weak SPP coupling ( $\Pi_{\text{SPP}} < 1.0$ ) the numerator plays a dominating role and that is why we have an enhancement. On the other hand, in the strong SPP coupling limit ( $\Pi_{\text{SPP}} > 1.0$ ) the denominator plays the dominating role and that is why the Kerr coefficient decreases.

We study the effect of the size and shape of MNS on the Kerr coefficient. The shape and size of MNS depends on the two quantities  $R_s$  and  $R_m$ , where  $R_s$  is the radius of

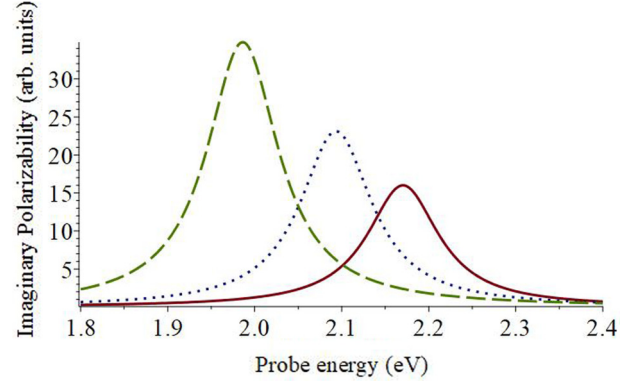


FIG. 9. The imaginary part of the polarizability factor ( $\zeta_s$ ) as a function of probe energy (eV) is plotted for a general nanohybrid. The solid, dotted, dash, and dash-dotted lines are plotted for the shape ratio  $R_m/R_s = 0.85$ ,  $R_m/R_s = 0.90$ , and  $R_m/R_s = 0.95$ , respectively.

the dielectric shell and  $R_m$  is the radius of the metallic core. In our theory, the SPP field and DDI field depend on the polarizability factor ( $\zeta_s$ ) as shown by Eq. (4) and Eqs. (7) and (8), respectively. The polarizability factor depends on  $R_s$  and  $R_m$  as shown in Eq. (2). Therefore, to show the effect of the  $R_s$  and  $R_m$  on the SPP field and the DDI field, we have calculated the polarizability factor for the MNS. The MNS is made of the  $\text{SiO}_2$  shell and a gold (Au) core. Cadmium-selenium quantum dots are considered as QEs. This type of nanohybrid is fabricated by Xiao *et al.* [39]. The effect of the shape ratio ( $R_m/R_s$ ) on the polarizability is plotted in Fig. 9. Here we have kept  $R_s$  as constant. In this figure, the imaginary part of the polarizability factor is plotted as a function of probe field energy (eV) for different values of the shape ratio. The solid, dotted, and dash lines are plotted for the shape ratio  $R_m/R_s = 0.85$ ,  $R_m/R_s = 0.90$ , and  $R_m/R_s = 0.95$ , respectively. One can see from the figure that as the shape ratio increases the height of the peak also increases. Note that the location of the peak of the polarizability factor also changes with the variation of the shape ratio. The location of the peak is nothing but the SPP resonance energy ( $\omega_{\text{sp}}$ ). It is important to note that we found the SPP resonance frequency changes with the change of the shape ratio.

We have established in Fig. 9 that the SPP resonance frequency ( $\omega_{\text{sp}}$ ) changes with the change of the shape ratio ( $R_m/R_s$ ). Therefore, the effect of the size and shape on the Kerr coefficient can be investigated via the SPP resonance frequency. The effect of the resonance frequency is included in the Kerr effect via the SPP detuning parameter  $\delta_s = \omega_{\text{sp}} - \omega_{23}$ . The results are shown in Fig. 10 where the Kerr coefficient is plotted as a function of the probe detuning for different SPP detunings. The solid and dotted lines are plotted for  $\delta_s = 0$ , and  $\delta_s = 0.5$  respectively. Here  $\delta_s = 0$  means that the SPP resonance frequency  $\omega_{\text{sp}}$  is in resonance with the exciton frequency  $\omega_{23}$  of the QE (i.e.,  $\omega_{\text{sp}} = \omega_{23}$ ). Note that the location of the crossing point shifts to the left when the SPP resonance frequency is not in resonance with the exciton energy (i.e., see the dotted line). This is consistent with the findings of Fig. 9 where we showed that as the shape ratio increases the peak of the polarizability shifts to the left. On the other

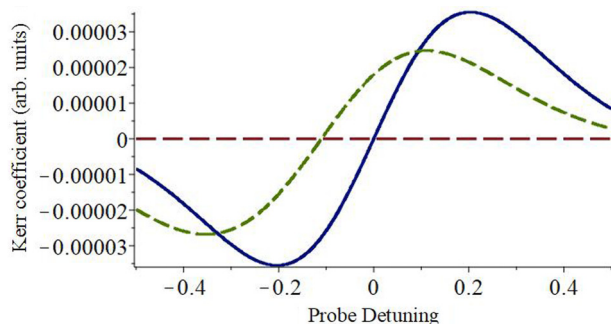


FIG. 10. The Kerr coefficient ( $n_2$ ) is plotted as a function of the probe detuning ( $\delta_p$ ). The solid and dotted lines are plotted for  $\delta s = 0.0$  and  $\delta s = 0.5$ , respectively.

hand, one can see that the height of both maxima decrease as the SPP resonance frequency is not in resonance with the exciton energy (i.e., see the dotted line). This is because the SPP coupling depends on the SPP resonance frequency via the polarizability factor. It is found that SPP coupling has the highest values when the SPP resonance frequency is in resonance with the exciton frequency. However, the SPP coupling is weak when they are not in resonance. That is why the peak height decreases in the case of the nonresonance condition.

## VI. CONCLUSIONS

In conclusion, we have developed a theory for the Kerr coefficient in nano hybrids made of an ensemble of metallic nanoshells and low concentration of quantum emitters. When the probe laser light falls in the metallic nanoshells, the surface plasmon polariton electric field is produced. This electric field along with the probe field induces dipoles in metallic nanoshells. These dipoles interact with each other via the dipole-dipole interaction. We found that in the weak SPP coupling limit, there is enhancement in the Kerr coefficient. On the other hand, in the strong SPP coupling limit, the peaks in the Kerr coefficient splits from two peaks to four peaks. The splitting in the Kerr spectrum is due to the presence of the dressed states created in the system due to the strong SPP interaction. These results are found when the SSP frequency is in resonance with exciton frequency. We showed that when the SPP frequency is not in resonance, the Kerr spectrum changes sign for one time to three times to five times.

## ACKNOWLEDGMENT

The author is thankful to the Natural Sciences and Engineering Research Council of Canada (NSERC) for a research grant.

- [1] M. Wersäll, J. Cuadra, T. J. Antosiewicz, S. Balci, and T. Shegai, *Nano Lett.* **17**, 551 (2016).
- [2] J. D. Cox, M. R. Singh, G. Gumbs, M. A. Anton, and F. Carreno, *Phys. Rev. B* **86**, 125452 (2012).
- [3] R. D. Artuso and G. W. Bryant, *Phys. Rev. B* **82**, 195419 (2010).
- [4] B. D. Fainberg, N. N. Rosanov, and N. A. Veretenov, *Appl. Phys. Lett.* **110**, 203301 (2017).
- [5] Y. Suganuma, P. E. Trudeau, B. Leathem, B. Shieh, and A. Dhirani, *J. Chem. Phys.* **118**, 9769 (2003).
- [6] X. Han, K. Wang, P. P. X. Xing, W. Liu, H. Long, F. Li, B. Wang, M. R. Singh, and P. Lu, *ACS Photon.* **7**, 562 (2020).
- [7] A. Terzis, S. Kosionis, J. Boviatsis, and E. Paspalakis, *J. Mod. Opt.* **63**, 451 (2016).
- [8] M. R. Singh, C. M. Sekhar, S. Balakrishnan, and S. Masood, *J. Appl. Phys.* **122**, 034306 (2017).
- [9] M. R. Singh, K. Davieau, and J. Carson, *J. Phys. D: Appl. Phys.* **49**, 445103 (2016).
- [10] M. R. Singh, D. Schindel, and A. Hatef, *Appl. Phys. Lett.* **99**, 181106 (2011).
- [11] M. M. Fejer, *Phys. Today* **47**(5), 25 (1994).
- [12] G. Cerullo and S. De Silvestri, *Rev. Sci. Instrum.* **74**, 1 (2003).
- [13] K. Sugioka, *Nanophotonics* **6**, 393 (2017).
- [14] E. O. Potma, W. P. De Boeij, and D. A. Wiersma, *J. Opt. Soc. Am. B* **17**, 1678 (2000).
- [15] V. Yannopapas and E. Paspalakis, *Phys. Rev. B* **97**, 205433 (2018).
- [16] M. M. Tohari, A. Lyras, and M. S. AlSalhi, *Nanomaterials* **8**, 521 (2018).
- [17] Q. Liu, X. He, X. Zhao, F. Ren, X. Xiao, C. Jiang *et al.*, *J. Nanopart. Res.* **13**, 3693 (2011).
- [18] K. L. Kelly, E. Coronado, L. L. Zhao, and G. C. Schatz, *J. Phys. Chem. B* **107**, 668 (2003).
- [19] M. R. Singh, *Nanotechnology* **30**, 205203 (2013).
- [20] H. Schmidt and A. Imamoglu, *Opt. Lett.* **21**, 1936 (1996).
- [21] H. Wang, D. Goorskey, and M. Xiao, *Phys. Rev. Lett.* **87**, 073601 (2001).
- [22] X. Yan *et al.*, *Phys. Lett. A* **372**, 6456 (2008).
- [23] H. Wang *et al.*, *Opt. Lett.* **27**, 258 (2002).
- [24] D. X. Khoa *et al.*, *J. Opt. Soc. Am.* **31**, 1330 (2014).
- [25] J. Ren *et al.*, *Nanotechnology* **27**, 425205 (2016).
- [26] L. V. Doal, D. X. Khoa, and N. H. Bang, *Phys. Scr.* **90**, 045502 (2015).
- [27] J. Sheng, X. Yang, H. Wu, and M. Xiao, *Phys. Rev. A* **84**, 053820 (2011).
- [28] C. Torres-Torres, A. López-Suárez, B. Can-Uc, R. Rangel-Rojo, L. Tamayo-Rivera, and A. Oliver, *Nanotechnology* **26**, 295701 (2015).
- [29] A. López-Suárez, R. Rangel-Rojo, C. Torres-Torres, A. Benami, L. Tamayo-Rivera, J. A. Reyes-Esqueda, J. C. Cheang-Wong, L. Rodríguez-Fernández, A. Crespo-Sosa, and A. Oliver, *J. Phys.: Conf. Ser.* **274**, 012145 (2011).
- [30] M. R. Singh and K. Black, *J. Phys. Chem. C* **122**, 26584 (2018).
- [31] M. R. Singh, J. Guo, E. Fanizza, and M. Dubey, *J. Phys. Chem. C* **123**, 10013 (2019).
- [32] M. R. Singh, J. Guo, and J. Chen, *J. Phys. Chem. C* **123**, 17483 (2019).
- [33] L. Novotny and B. Hecht, *Principle of Nano-optics* (Cambridge University Press, Cambridge, UK, 2006), p.266, Sec. 8.3.3.

- [34] D. Sarid and W. A. Challener, *Modern Introduction to Surface Plasmons: Theory, Mathematica Modeling, and Applications* (Cambridge University Press, New York, 2010).
- [35] E. Hamura, Y. Kawabe, and A. Yamanaka, *Quantum Nonlinear Optics* (Springer, Tokyo, 2007), Chap. 6.
- [36] R. W. Boyd, *Nonlinear Optics*, 3rd ed. (Academic, New York, 2008), Chap. 2.
- [37] M. R. Singh, *Electronic, Photonic, Polaritonic and Plasmonic Materials* (Wiley Custom, Toronto, 2014).
- [38] M. O. Scully and M S Zubairy, *Quantum Optics* (Cambridge University Press, London, 1997).
- [39] S. Xiao, H. Gong, X. Su, J. Han, Y. Han, M. Chen, and Q. Wang, *J. Phys. Chem. C* **111**, 10185 (2007).